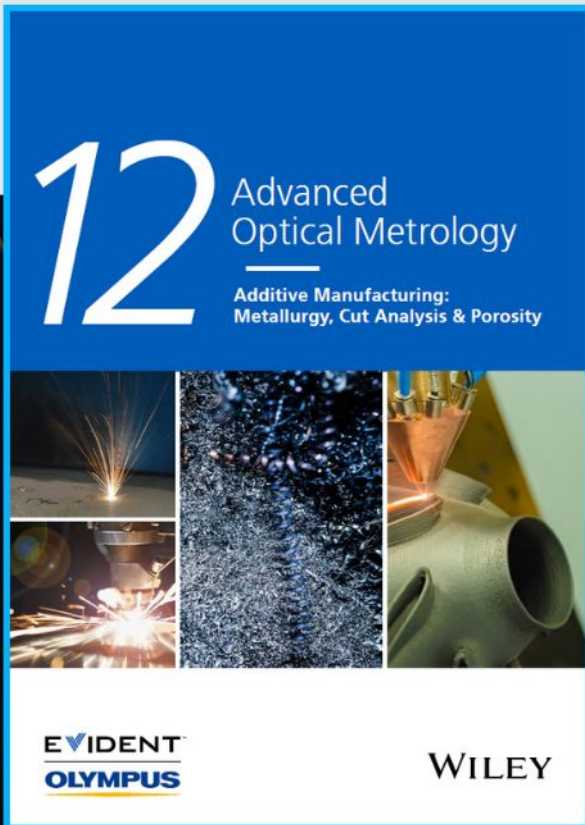




Additive Manufacturing: Metallurgy, Cut Analysis & Porosity



The latest eBook from
Advanced Optical Metrology.
Download for free.

In industry, sector after sector is moving away from conventional production methods to additive manufacturing, a technology that has been recommended for substantial research investment.

Download the latest eBook to read about the applications, trends, opportunities, and challenges around this process, and how it has been adapted to different industrial sectors.

EVIDENT™
OLYMPUS

WILEY

Local Heating Transforms Amorphous Calcium Carbonate to Single Crystals with Defined Morphologies

Shuheng Zhang, Ouassef Nahi, Xuefeng He, Li Chen, Zabeada Aslam, Nikil Kapur, Yi-Yeoun Kim, and Fiona C. Meldrum*

The use of amorphous calcium carbonate (ACC) as a precursor phase affords organisms with outstanding control over the formation of calcite and aragonite biominerals. Essential to this strategy is that the ACC is maintained within confined volumes in the absence of bulk water. This ensures that the ACC undergoes a pseudomorphic transformation and that the organism can independently control nucleation and growth. However, comparable control has proven hard to achieve in synthetic systems. Here, a straightforward method is demonstrated for controlling the crystallization of ACC thin films in which nucleation is first triggered using a heated probe, and then growth is sustained by incubating the film at a lower temperature. By independently controlling nucleation and growth, sub-millimeter calcite single crystals can be generated when and where it is desired, morphologies ranging from discs to squares to serpentine strips can be created, and arrays of crystals formed. The mechanism and energetics of crystallization of the ACC are studied using in situ transmission electron microscopy and continuity between the ACC and calcite at the growth front is demonstrated. It is envisaged that this method can be applied to the formation of large single crystals of alternative functional materials that form via amorphous precursor phases.

1. Introduction

The study of biomineralization processes has delivered many strategies for controlling crystallization in synthetic systems.^[1,2] One of the most influential is the use of amorphous precursor phases, which afford organisms greater control than an ion-by-ion growth mechanism. This can be seen in the extensively studied calcium carbonate system, where amorphous calcium carbonate (ACC) acts as a precursor to calcite^[3–5] and aragonite^[6–8] and enables rapid crystallization, the creation of non-crystallographic morphologies^[9,10] and the formation of large single crystals.^[11] Key to this control is that mineralization in biological systems invariably occurs within privileged environments.^[12] This ensures that the ACC phase is maintained in the presence of limited water,^[3] such that the transformation occurs in the solid state and the morphology of the precursor ACC material is preserved in the product crystal.^[13]

This basic principle has been translated to synthetic systems by entrapping ACC within confined volumes,^[9,10,14] crystallizing dry ACC under humid conditions,^[15,16] and by heating ACC.^[17–19] In this way it has proven possible to form crystalline thin films with mosaic-type structures,^[20–22] to generate single crystals with non-crystallographic morphologies,^[9,10,14] and create composite materials.^[23,24] Liu et al. developed a process in which calcite single crystals with various morphologies could be generated after removing the solvent from triethylamine-capped calcium carbonate oligomers generated in ethanol.^[25] However, defining the structure and morphology of the product crystals in these systems remains challenging, particularly for ACC generated in aqueous solution. Course control over crystal morphology has also been gained when ACC monoliths with defined water contents were placed under external pressure.^[26]

As shown to great effect by biology, superior control over crystallization can be achieved by independently controlling both nucleation and growth. This is again easier to accomplish with an ACC precursor than ion-by-ion growth, where ACC can be long-lived when confined in small volumes,^[27] giving organisms the opportunity to define when and where nucleation occurs. This principle has been demonstrated in the formation of large calcite single crystals via the room-temperature

S. Zhang, O. Nahi, X. He, Y.-Y. Kim, F. C. Meldrum
School of Chemistry
University of Leeds
Woodhouse Lane, Leeds LS2 9JT, UK
E-mail: f.meldrum@leeds.ac.uk

L. Chen
School of Electronic and Electrical Engineering
University of Leeds
Woodhouse Lane, Leeds LS2 9JT, UK

Z. Aslam
School of Chemical and Process Engineering
University of Leeds
Woodhouse Lane, Leeds LS2 9JT, UK

N. Kapur
School of Mechanical Engineering
University of Leeds
Woodhouse Lane, Leeds LS2 9JT, UK

 The ORCID identification number(s) for the author(s) of this article can be found under <https://doi.org/10.1002/adfm.202207019>.

© 2022 The Authors. Advanced Functional Materials published by Wiley-VCH GmbH. This is an open access article under the terms of the Creative Commons Attribution License, which permits use, distribution and reproduction in any medium, provided the original work is properly cited.

DOI: 10.1002/adfm.202207019

transformation of ACC thin films in solution when a nucleation site was pre-formed on the supporting substrate.^[28]

Here, we present a simple and versatile strategy for fabricating large single crystals of calcite with arbitrary morphologies from an ACC precursor phase. Nucleation is triggered at a single point in an ACC thin film using a heated probe, and then growth is sustained – in the absence of further nucleation – by uniform heating at a lower temperature. We can therefore determine when and where nucleation occurs, and control growth to generate sub-millimeter single crystals of calcite, as compared with the micro-sized mosaic structures formed without triggered nucleation.^[29–31] Indeed, dry ACC can be stabilized for months depending on its composition. This method is considerably more flexible than using surface chemistry to initiate nucleation,^[11] when the nucleation site has to be built into the system such that the transformation begins the moment the ACC is deposited. Our strategy is also readily extended to generate arrays of single crystals, and the mechanism of ACC crystallization can be studied using in situ transmission electron microscopy (TEM).

2. Results

2.1. Formation of ACC Thin Films

Uniform, large area ACC thin films were formed via a polymer-induced liquid precursor (PILP) process using the ammo-

ni-um diffusion method (ADM).^[32,33] Substrates including silicon wafers and TEM grids were placed at the base of 10 mm × 10 mm × 1 mm reaction wells that were then covered with a thin film of gas-permeable poly(dimethylsiloxane) (PDMS). Reaction solutions containing [CaCl₂] = 10 mM, [MgCl₂] = 4–100 mM, and poly(acrylic acid) (PAA) = 4 μg mL⁻¹ were injected into the wells, and exposed to ammonium carbonate vapor, leading to the formation of ACC thin films on the substrates (Figure 1a). These conditions were selected as they generate high-quality thin films.^[34] The substrates were then removed from the solution and the ACC films were rinsed with ethanol and dried with nitrogen gas. The product films exhibited uniform blue interference colors and their amorphous structure was confirmed by the absence of birefringence using polarized optical microscopy (POM) and selected area electron diffraction (SAED) (Figure 1b–d). Atomic force microscopy (AFM) demonstrated thickness of ≈100 nm (Figure S1, Supporting Information).

The presence of PAA and Mg²⁺ ions was essential to the uniformity and continuity of ACC films, where they increase the coalescence of the ACC particles and their ability to wet the substrate.^[20,35] In contrast, continuous films could not be formed under additive-free conditions. The deposition times were also optimized such that uniform ACC films formed, as exemplified with films prepared after 30 min from a solution comprising [Mg²⁺] = 4 mM and [PAA] = 4 μg mL⁻¹ (Figure S2, Supporting Information). Extended times resulted in the formation of crystalline particles in solution, which incorporate

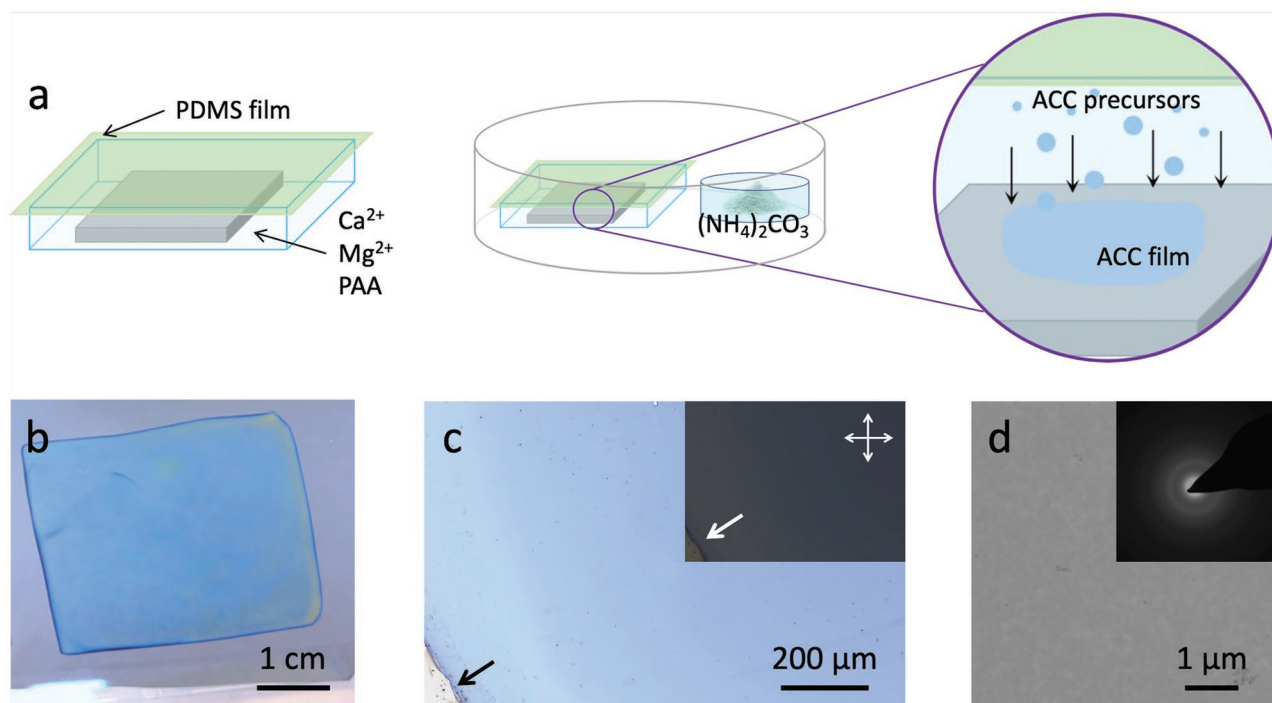


Figure 1. Synthesis and characterization of ACC films. a) Schematic diagram of the process used to deposit the ACC films on silicon. A silicon substrate was placed in a 1 mm deep PDMS reaction well. This was then covered by a gas permeable PDMS film and filled with the reaction solution. The reaction well was placed in a sealed Petri dish with (NH₄)₂CO₃ powder, generating ACC particles that coalesce to a thin film on the substrate. b) Micrograph of a large ACC film (3 cm × 4 cm) generated under conditions [Ca²⁺] = [Mg²⁺] = 10 mM, [PAA] = 4 μg mL⁻¹, where the film shows a blue interference color. c) Bright-field optical micrograph of the ACC films with (inset) a corresponding POM image showing no birefringence. The black arrow indicates the edge of the ACC film. d) Bright-field TEM image and corresponding SAED (inset) of the ACC film, revealing no crystallinity.

into the ACC films and then grow at the film's expense. A range of contrasting substrates including glass, silicon, PMMA (poly(methyl methacrylate)), PVA (poly(vinyl acetate)), and PDMS were tested and high-quality films were obtained on all, showing that the substrate has little influence on film formation (Figure S3, Supporting Information).

2.2. Solid-State Transformation of ACC Films

The crystallization behavior of the ACC films was then investigated. Dry ACC films can crystallize at room temperature and

ambient humidity at a rate that is dependent on their composition, demonstrating that this is a kinetically-controlled process. Films prepared at $[Mg^{2+}] = 10 \text{ mM}$ and $[PAA] = 4 \mu\text{g mL}^{-1}$ crystallized within 9–15 h, as compared with 1–3 days when $[Mg^{2+}]$ is raised to 20 mM. Extremely stable ACC films could be generated with $[Mg^{2+}] = 50\text{--}100 \text{ mM}$ such that no crystallization was observed within 30–60 days. All films that crystallized at room temperature comprised birefringent, spherulitic domains as viewed using POM, and their polymorphs were polycrystalline calcite as identified by SAED (Figure 2a–c).

In contrast, excellent control over nucleation could be achieved by heating the ACC films. The films were heated

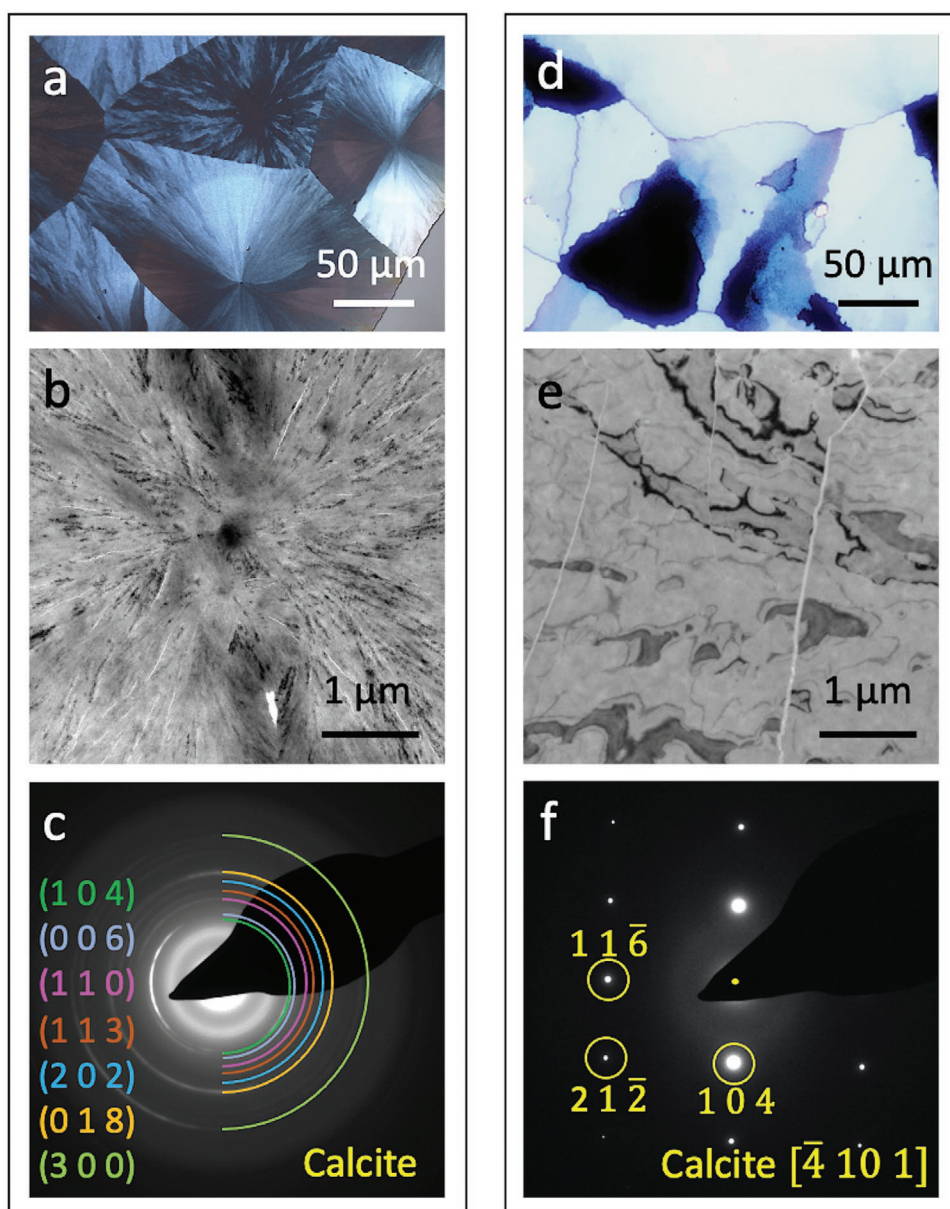


Figure 2. Crystallization of ACC films generated under conditions $[Ca^{2+}] = [Mg^{2+}] = 10 \text{ mM}$, $[PAA] = 4 \mu\text{g mL}^{-1}$. a) POM image of spherulitic calcite film formed after storing the ACC film for 3 days at ambient conditions. b) Bright-field TEM image and c) corresponding SAED pattern of the polycrystalline spherulitic domains. d) POM image of the single-crystal domains formed by crystallizing ACC film at $150 \text{ }^\circ\text{C}$ (T_{ON}) for 5 h. e) Bright-field TEM image and f) corresponding SAED pattern of a single-crystal calcite domain.

at a rate of $10\text{ }^{\circ}\text{C min}^{-1}$ and the onset nucleation temperature (T_{ON}) at which nucleation was first observed was identified from the emergence of birefringence in polarized optical microscopy. T_{ON} varied according to the composition of the film, being $220\text{ }^{\circ}\text{C}$ for films prepared at $[\text{Mg}^{2+}] = 15\text{ mM}$ and $[\text{PAA}] = 4\text{ }\mu\text{g mL}^{-1}$, and $150\text{ }^{\circ}\text{C}$ for preparation conditions of $[\text{Mg}^{2+}] = 10\text{ mM}$ and $[\text{PAA}] = 4\text{ }\mu\text{g mL}^{-1}$. Films prepared at $[\text{Mg}^{2+}] = 10\text{ mM}$ and with no presence of PAA crystallized at $140\text{ }^{\circ}\text{C}$, demonstrating that the Mg^{2+} ions had a much greater effect on T_{ON} than PAA. Values of T_{ON} were highly reproducible, varying by only $\pm 5\text{ }^{\circ}\text{C}$. Continued incubation of the ACC films at T_{ON} resulted in nucleation at random sites, such that the ACC transformed into a mosaic of single crystal calcite domain (Figures 2d–f and Movie S1, Supporting Information).

These values can be compared with values determined for bulk ACC samples using thermogravimetric analysis (TGA). The latter has shown that ACC crystallization in the solid state often takes place at $\approx 300\text{--}330\text{ }^{\circ}\text{C}$,^[36–41] although significantly lower values of $200\text{ }^{\circ}\text{C}$ ^[41] and even $105\text{ }^{\circ}\text{C}$ ^[42] have been reported. The temperature is primarily determined by the pH at which the ACC was precipitated,^[41,43] where ACC formed at high pH values contains more hydroxyl ions, and crystallizes at higher temperatures. The crystallization temperature is also dependent on the particle size, and is higher for small particles.^[44,45] This is attributed to their lower water content.^[45]

2.3. Analysis of the Transformation Mechanism

Further insight into the nucleation process was gained using in situ TEM. Exemplifying with ACC films prepared

under standard conditions $[\text{Ca}^{2+}] = [\text{Mg}^{2+}] = 10\text{ mM}$ and $[\text{PAA}] = 4\text{ }\mu\text{g mL}^{-1}$, the films were deposited on SiN TEM window grids and were then heated to $T_{\text{ON}} = 150\text{ }^{\circ}\text{C}$ to generate a small number of nuclei. Sequential bright field TEM images of the growing nuclei were then recorded during uniform heating at $130\text{ }^{\circ}\text{C}$ (below T_{ON}) (Figure 3a). The growth front propagated at a rate of $15\text{--}25\text{ nm sec}^{-1}$ and a direct transformation of the ACC to a single crystal occurred with no further nucleation, cracking, or shrinking, as demonstrated by the presence of continuous bend contours. High-resolution transmission electron microscopy (HRTEM) images and corresponding fast Fourier transform (FFT) pattern further confirmed the presence of single crystals of calcite (Figure 3b). The non-uniform appearance of this sample in the HRTEM images is due to minor beam damage, which is very common in these beam-sensitive samples.

Investigation of the chemical compositions of the ACC and calcite films at the interfacial region using high-angle annular dark field scanning TEM with energy dispersive X-ray analysis (HAADF-STEM EDX) showed that Mg was uniformly distributed in both phases with compositions of $9.3 \pm 2.1\text{ mol}\%$ and no depletion or enrichment was observed at their interface (Figure S4, Supporting Information). Inductively coupled plasma/optical emission spectrometry (ICP-OES) further showed that the precursor ACC films contained $10.0 \pm 0.3\text{ mol}\%$ Mg. This continuity in Mg levels is expected for a solid-state transformation.^[46]

Given the uniform propagation of the growth front, the temperature dependence of the rate of crystallization of the ACC films provides information about the activation energy associated with the growth of crystalline phases from ACC.^[47,48] The

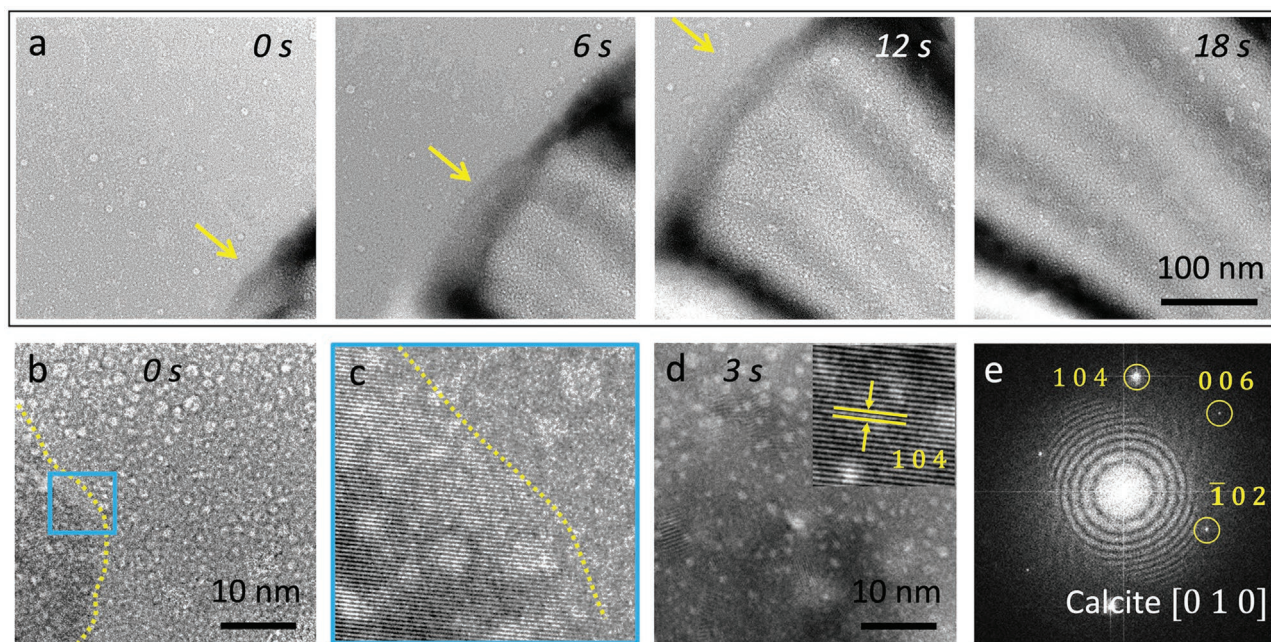


Figure 3. Transformation of ACC films with in-situ heating during TEM at $130\text{ }^{\circ}\text{C}$. The ACC films were produced at $[\text{Ca}^{2+}] = [\text{Mg}^{2+}] = 10\text{ mM}$, $[\text{PAA}] = 4\text{ }\mu\text{g mL}^{-1}$ and possess $T_{\text{ON}} = 150\text{ }^{\circ}\text{C}$. a) Sequential micrographs of the transformation of ACC films, where the yellow arrows indicate the advancing growth front. Dose rate = $39\text{ e }^{\text{Å}}^{-2}\text{ s}^{-1}$. b–e) HRTEM micrographs of the transforming ACC film. Dose rate = $409\text{ e }^{\text{Å}}^{-2}\text{ s}^{-1}$. b,c) The crystal front at 0 s (indicated by the yellow dashed lines), where (c) corresponds to the blue square in (b). The domain imaged in (c) fully transforms to a single crystal of calcite after 3 sec . The inset in (d) shows lattice fringes corresponding to the $\{104\}$ set of planes and (e) shows the corresponding FFT diffractogram.

overall reaction kinetics of the solid-state transformation of ACC at a given temperature can be described by an Arrhenius type equation (Equation 1).^[49]

$$\beta = n_0 \exp\left(-\frac{E_c}{RT}\right) \quad (1)$$

where E_c is the activation energy, R is the ideal gas constant, T is the temperature, and ν_0 is a constant frequency factor. β is the rate of propagation of the growth front ($\mu\text{m sec}^{-1}$, Table S1, Supporting Information). A plot of $\ln\beta$ versus $1/T$ reveals a linear relationship, from which activation energy of 113 kJ mol^{-1} can be extracted (Figure S5, Supporting Information).

This value can be compared with activation energies of 73 kJ mol^{-1} and 66 kJ mol^{-1} for calcite nucleation and growth in solution,^[50] and 70 kJ mol^{-1} for calcite formation^[51] in aqueous solution. The formation of calcite from ACC in the solid state is associated with a larger activation energy, where values of 100 kJ mol^{-1} ,^[52] and $151\text{--}304 \text{ kJ mol}^{-1}$ ^[36] have been derived for the formation of calcite from ACC in the solid state. The values of 151 kJ mol^{-1} and 304 kJ mol^{-1} were obtained for ACC precipitated at pH 12.2 and 13, respectively. Activation energies of 245 kJ mol^{-1} have additionally been derived for the loss of the final water fraction from additive-free ACC^[52] prior to nucleation, demonstrating that high temperatures are required if ACC is to fully dehydrate prior to crystallization.

The kinetics of crystallization is also dependent on the thickness of the ACC film. This was observed by depositing an ACC film on a tilted substrate, which gives rise to a film whose thickness varies according to the location on the substrate (Figure S6, Supporting Information). Thinner areas of the film crystallized at a higher onset temperature than their thicker counterparts and lower growth rates were observed for thinner films at a given temperature. This can be attributed to reduced ion mobility in thinner films which stabilizes the ACC film,^[47] and is consistent with classical nucleation theory that predicts that the nucleation frequency decreases with a decreasing volume of material.^[53]

2.4. Triggering Transformation to Large Single Crystals

Having established control over nucleation, large single crystals could be generated by further developing this method to independently control nucleation and growth. This was achieved using a two-step method in which (i) nucleation was triggered at a single site using a hot probe held at a temperature exceeding T_{ON} , and (ii) growth of the nucleus was sustained by uniform heating below T_{ON} . Incubation below T_{ON} resulted in a much longer induction time for the birth of new nuclei such that they could not be formed within the experimental time frame. This strategy was demonstrated by gently tapping an ACC film prepared under standard conditions with a probe held at $180 \text{ }^\circ\text{C}$ ($\gg T_{\text{ON}}$) (Figure S7, Supporting Information). Nucleation occurred in $<1 \text{ sec}$, resulting in the formation of a single birefringent spot (Figure 4a and Movie S2, Supporting Information). Subsequent incubation at $130 \text{ }^\circ\text{C}$ ($< T_{\text{ON}}$) then allowed the nucleus to grow in

the absence of any further nucleation events (Movie S3, Supporting Information), resulting in the formation of large single crystals $\approx 0.5 \text{ mm}$ in size. The crystals possessed the same thicknesses and morphologies as the original ACC film (Figures S1 and S8, Supporting Information), and SAED and HRTEM confirmed that they were single crystals of calcite (Figure 4b,c).

2.5. Controlling Crystal Morphologies

This methodology can be readily adapted to create patterned single crystals and arrays of crystals with any desired shape by employing patterned substrates. Individual calcite single crystals perforated by a periodic array of holes were formed by depositing ACC films on a silicon wafer patterned with an array of $20\text{--}30 \mu\text{m}$ diameter micro-posts that are set $20\text{--}50 \mu\text{m}$ apart (Figure 5a). Subsequent lift-off of the posts yielded patterned millimeter-scale ACC films (Figure 5b,c). Transformation of these films at room temperature generated spherulitic structures identical to those seen for unpatterned films under the same conditions (Figure 5d and Figure S8a, Supporting Information), while single crystal domains formed if the film was incubated at T_{ON} (Figure 5e). Application of the 2-step method, in contrast, yielded large, single crystals perforated by the holes defined by the posts (Figure 5f and Figure S9b, Supporting Information). Formation of these structures was followed using POM, and the growth front could be seen to bifurcate and then encircle the pillars, before rejoining seamlessly on the other side (Movie S4, Supporting Information).

Arrays of single crystals with specific sizes, shapes, and configurations were also generated on substrates that had been lithographically-patterned with arrays of the desired shape (Figure 6a). Patterned substrates were fabricated by spin-coating a layer of photoresist on silicon wafers, exposing to UV light through a suitable mask, and developing to remove the uncured photoresist. ACC then deposits preferentially on the exposed hydrophilic silicon, and subsequent lift-off of the photoresist creates an array of ACC domains on the substrate (Figure 6b).

Small domains of ACC could be directly transformed to calcite single crystals in a single step by incubating the substrate at an elevated temperature. Exemplifying with an array of $10 \mu\text{m}$ diameter ACC discs, these transform into single crystals by uniform heating at $200 \text{ }^\circ\text{C}$ (Figure 6c, Movie S5, Supporting Information). Although this temperature far exceeds T_{ON} , the balance between the nucleation and growth rates is such that the ACC in each domain crystallizes before a second nucleation event can occur. A comparable result was obtained on transforming ACC stripes that were $10 \mu\text{m}$ in width and set $50 \mu\text{m}$ apart at $200 \text{ }^\circ\text{C}$ (Figure 6d). Larger single crystals with arbitrary morphologies could be generated using our 2-step method. Figure 7 shows examples of single crystals with sizes of $\approx 500 \mu\text{m}$ and shapes including discs, squares, hexagons, and serpentine stripes, where these were produced using nucleation and growth temperatures of $180 \text{ }^\circ\text{C}$ ($\gg T_{\text{ON}}$) and $120 \text{ }^\circ\text{C}$ ($< T_{\text{ON}}$), respectively. In contrast, spherulitic structures formed if the ACC films were simply incubated under ambient conditions.

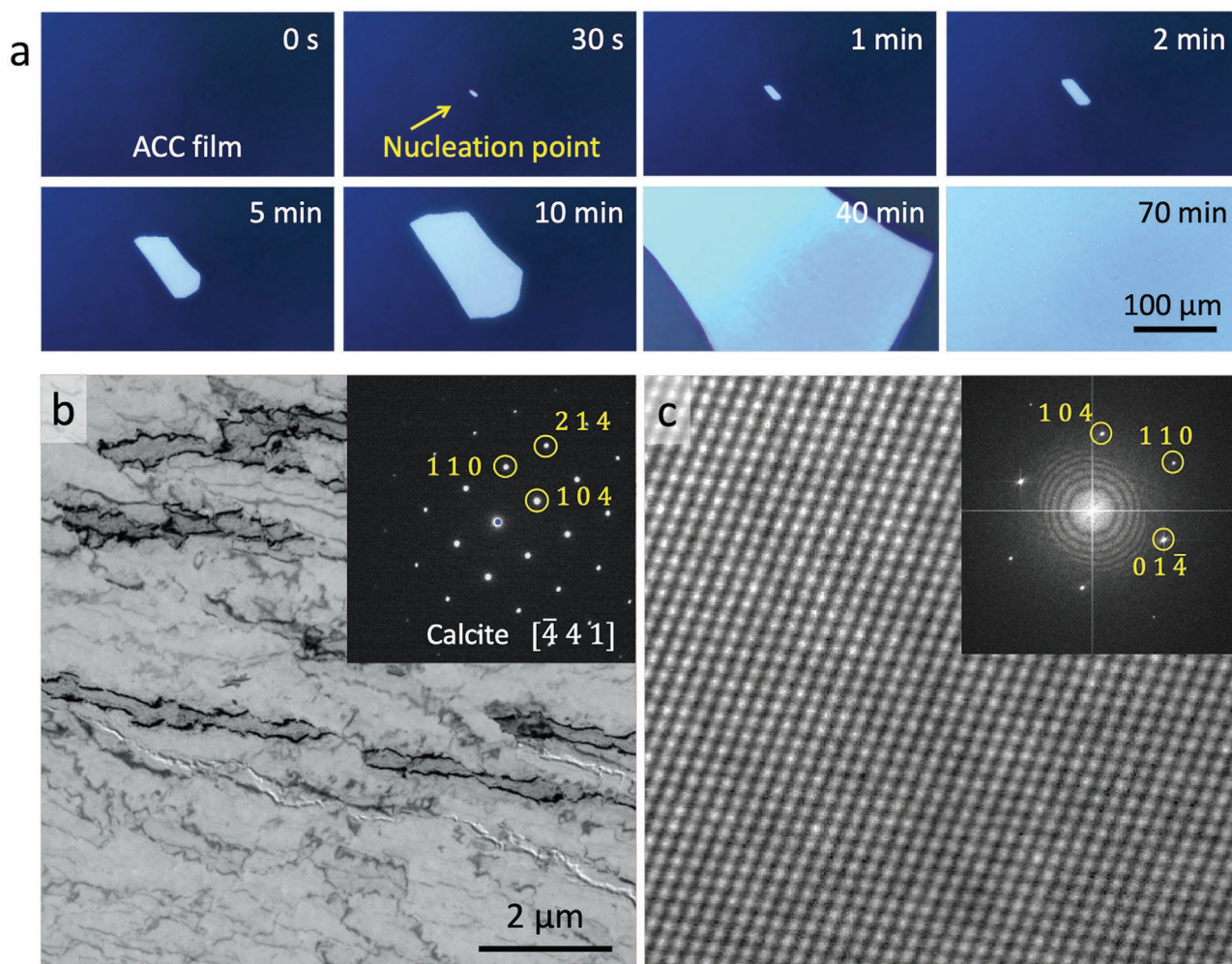


Figure 4. Production of large single crystals of calcite, where nucleation was triggered at a single site with a heated probe, and the film was then uniformly heated at 130 °C. The ACC films were produced at $[Ca^{2+}] = [Mg^{2+}] = 10$ mM, $[PAA] = 4 \mu\text{g mL}^{-1}$ and possess $T_{ON} = 150$ °C. a) Sequential POM micrographs showing the initial ACC precursor film at 0 s, the nucleation point, where the image was recorded after 30 s, when it was large enough to be viewed with a microscope, and continued transformation of the ACC film. b) Bright field TEM image and corresponding SAED pattern (inset) of the product single-crystal calcite film. c) HRTEM image and corresponding FFT diffractogram.

3. Discussion

Crystallization via an ACC precursor phase enables organisms to generate large single crystals with complex morphologies. But appealing as this strategy may be, it has proven challenging to translate to synthetic systems. As also occurs in biomineralization, single crystals with complex shapes or non-crystallographic morphologies can be generated by a pseudomorphic transformation of ACC using a templating approach. However, this requires that the template is fully filled with the amorphous precursor phase. It is not yet clear how organisms achieve this, but they have the means to translocate particles or ions into the privileged environments in which crystallization will occur.^[54,55]

As simple precipitation of ACC, even from highly concentrated solutions, results in a gel-like phase that is not space-filling,^[27] synthetic methods have adopted strategies where the ACC is concentrated within the template using a filtration method,^[56] or through physical compression.^[57] These often

require the precise regulation of the external pressure, the water content of the ACC, and the nature and concentration of additive.^[15,26] In a very different approach, large quantities of a moldable precursor phase could be generated by precipitating calcium carbonate from ethanol solutions containing triethylamine (TEA), which was then crystallized by heating to drive off the TEA.^[25]

The challenge of completely filling the template with the precursor phase can also be overcome using a precursor with liquid-like properties, where PILP phases have also been postulated to operate in biological systems.^[32] Calcite single crystals with rod-like morphologies and diameters of up to a few hundred nanometres have been generated by filling a template with a PILP phase,^[10] while gyroid structures with 50 nm pores^[9] have been formed by filling structured polymer templates with ACC precipitated in the presence of methanol. However, it is hard to produce significant quantities of the precursor phase using these approaches and attempts to scale-up the PILP

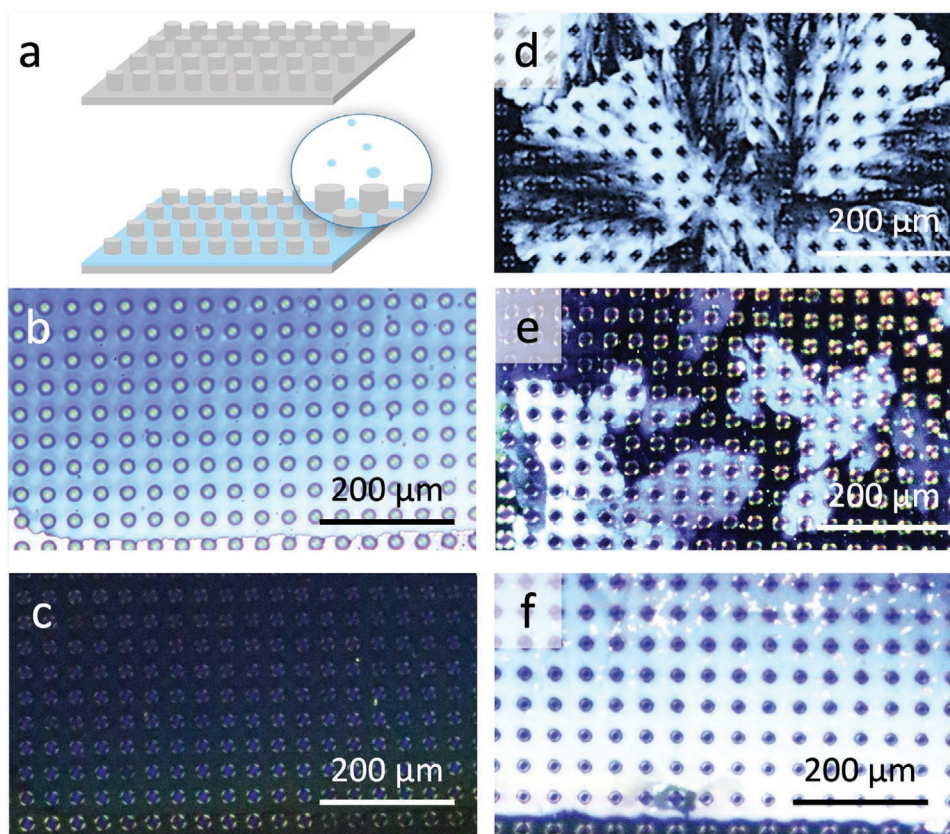


Figure 5. a) Micropatterned calcite films generated by depositing ACC films on silicon substrates patterned with photoresist microposts that are 20 μm in diameter, 2 μm in height, and set 20–50 μm apart. b) OM and c) POM images of the patterned ACC film. d,e) Transformation of micropatterned ACC films (d) at room temperature and (e) with uniform heating at T_{ON} (140 $^{\circ}\text{C}$). f) Single crystal formed with the two-step control strategy. The ACC films were formed from solutions comprising $[\text{Ca}^{2+}] = 10 \text{ mM}$, $[\text{Mg}^{2+}] = 4 \text{ mM}$ and $[\text{PAA}] = 4 \mu\text{g mL}^{-1}$. All micrographs are shown at the same magnification.

process using higher concentrations of polyelectrolyte generated a polycrystalline product.^[58]

The liquid-like properties of a PILP phase are particularly well-suited to the formation of thin films. Following the formation of a continuous thin film of PILP on a substrate, these typically crystallize in solution to give a mosaic of spherulitic and single crystal domains that are 50–150 μm in size and irregular in morphology.^[20,29,31] The size of the domains is governed by the balance between the nucleation and growth rates, where this can be controlled to some degree by the composition of the PILP^[20] and the nature of the substrate.^[21,59]

To achieve a high level of control over ACC crystallization – as is required to generate single crystals with specific morphologies – it is therefore necessary to separately control nucleation and growth. This is challenging in aqueous systems, but has been achieved in a system where an ACC film was deposited on a substrate patterned with an array of pillars.^[11] A single nucleation site was defined on the substrate prior to depositing the ACC, which then transformed to calcite single crystals with sizes of up to 500 μm . However, this was only achieved when the pillars were separated by 15 μm or less, where it was speculated that these acted as sites to release water and thus prevent a build-up of stress.

The solid-state system described here therefore enables excellent control over the crystallization of ACC, and pro-

vides some significant advantages over the above aqueous-based system, where (1) nucleation is external to the system and is not triggered until desired, and (2) both solid and internally-patterned calcite single crystals can be readily formed. The latter may derive from the low water content of the heated ACC films prior to nucleation and growth, where 75–85% of the water is lost by $\approx 150 \text{ }^{\circ}\text{C}$.^[38,41,52] Therefore, while ACC must expel significant quantities of water when crystallizing under ambient conditions, crystallization temperatures of $\approx 150 \text{ }^{\circ}\text{C}$ ensure that the ACC films only contain $\approx 20\%$ water. Indeed, it is possible that different transformation mechanisms operate under these conditions. Pseudomorphic transformation of ACC (of powders under humid conditions or thin films) occurs at room temperature because there is sufficient water present to facilitate nucleation via local dissolution/ reprecipitation.^[15,16] The water is then expelled as the transformation progresses, potentially through continuous local dissolution/ reprecipitation.^[15] Under the high temperature conditions employed here, it is postulated that nucleation occurs by an internal structural reorganization within the ACC. The continuity at the interface between the ACC and calcite, as viewed using TEM, then again suggests a solid-state transformation in which the remaining water may be expelled at the large surfaces of the thin film.

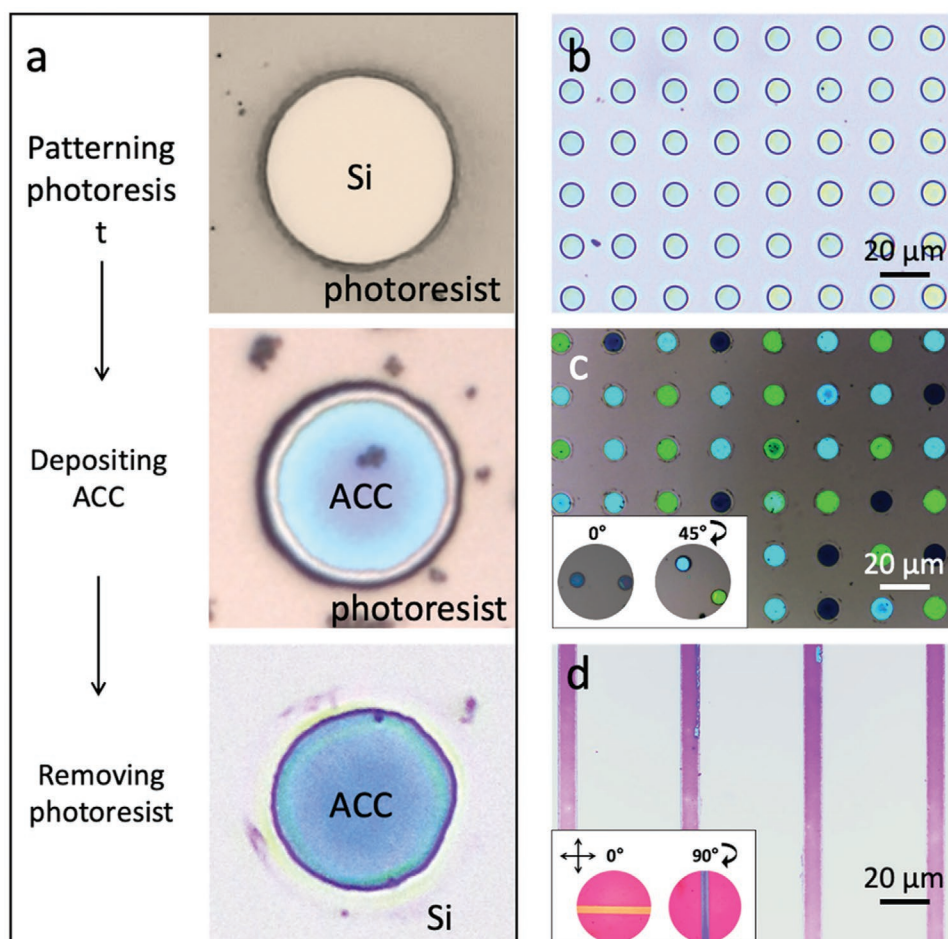


Figure 6. Creation of single crystal calcite arrays. a) A silicon substrate was coated with a layer of photoresist containing an array of circular holes. ACC preferentially forms within the holes, giving an array of ACC discs after lift-off of the photoresist. b) Optimal micrograph of an array of ACC discs that are 10 μm in diameter and set 15 μm apart. c) POM image recorded after heating the sample in (b) at 200 $^{\circ}\text{C}$. The insets show a uniform change in the polarization color on rotation of the specimen stage. d) OM image of calcite stripes that are 10 μm in width and set 50 μm apart. The inset is a full-wave-plate POM image showing a uniform change in polarization colors with rotation of the specimen stage, indicative of single crystal character. The ACC films were deposited from solutions comprising $[\text{Ca}^{2+}] = 10 \text{ mM}$, $[\text{Mg}^{2+}] = 4 \text{ mM}$, and $[\text{PAA}] = 4 \mu\text{g mL}^{-1}$.

4. Conclusion

Separately controlling nucleation and growth forms the basis of traditional techniques for generating large, high purity single crystals.^[60,61] It also enables organisms to generate structures such as nacre, and sea urchin larval spicules from an ACC precursor phase. We have here demonstrated that excellent control can be achieved over the transformation of ACC when the reaction is performed in the solid state, enabling the formation of millimeter-scale single crystals of calcite with a free choice of morphology. The approach is straightforward and delivers a degree of control that is difficult to achieve when ACC crystallizes in aqueous solution. Our system also enables the solid-state transformation of ACC to be imaged on the nanoscale, providing insight into the mechanism of crystallization of ACC. Finally, it is interesting to compare the structural control achieved in ACC-based systems with that obtained in ion-by-ion growth. While it is hard to envisage a method of preparing crystals with the sizes and shapes produced here in the absence of an amorphous phase, morphologically complex

3D calcite single crystals with sizes of a few hundred microns have been synthesized via ion-by-ion pathways using templating approaches.^[62,63] This far exceeds any dimension that has been achieved by a PILP route, although the latter excels when infiltration of mineral into small volumes is required.^[23] Nevertheless, an ion-by-ion approach is both slow and hard to control, where the ultimate crystal sizes again depend on the balance between nucleation and growth rates. Future work will therefore address strategies that enable space-filling by an ACC precursor, where these therefore promise the greatest potential control, and could be readily transformed using our approach to yield large 3D single crystals.

5. Experimental Section

Materials: Analytical grade $(\text{NH}_4)_2\text{CO}_3$, $\text{CaCl}_2 \cdot 2\text{H}_2\text{O}$, $\text{MgCl}_2 \cdot 6\text{H}_2\text{O}$, poly(acrylic acid) sodium salt (PAA, M_w 8000, 45 wt.%) were purchased from Sigma-Aldrich (UK) and used as received. Deionized Milli-Q water (18.2 $\text{m}\Omega\text{cm}$) was used for the preparation of precipitation solutions. Silicon <100> wafers were purchased from Inseto limited and used as

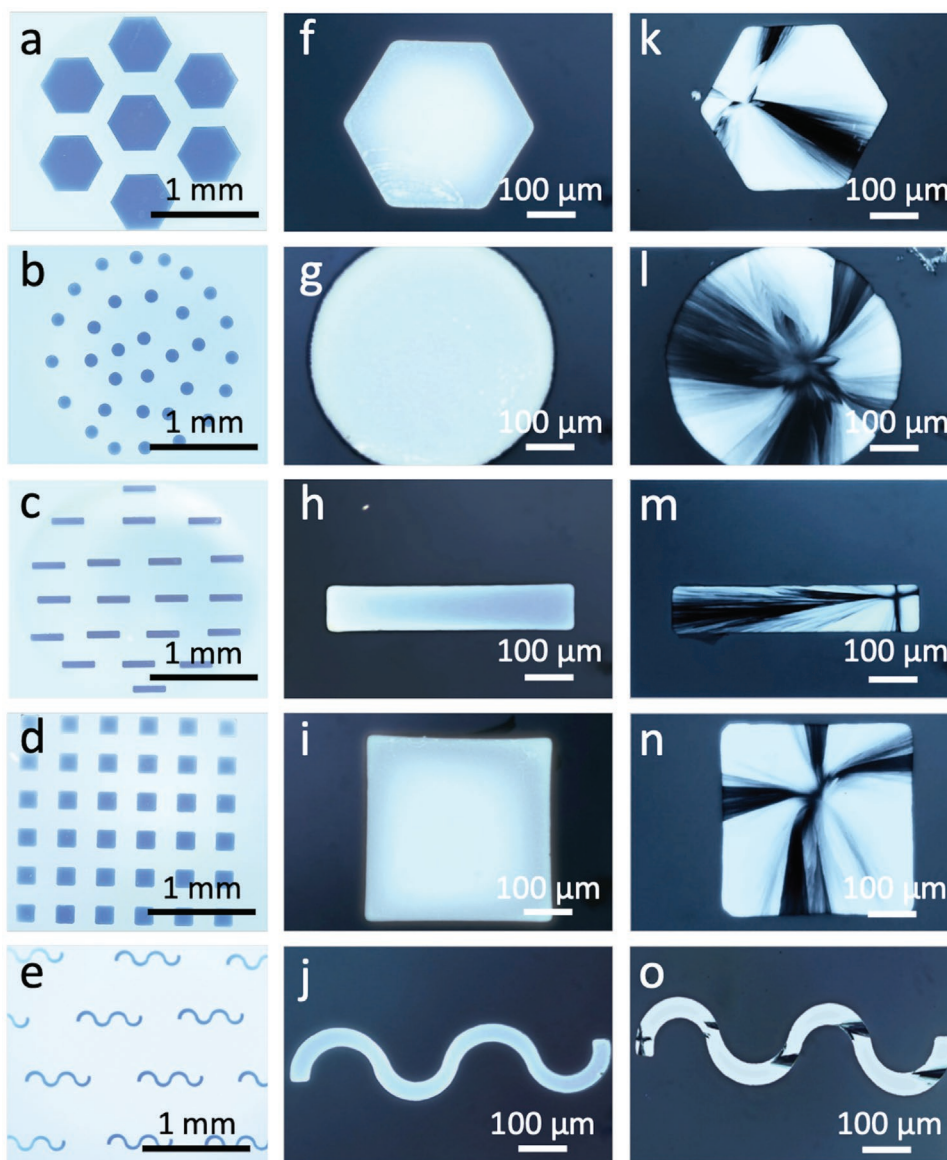


Figure 7. Creating large single crystals with arbitrary morphologies. OM images of a–e) large ACC films with shapes including hexagons, circles, stripes, squares, and serpentine stripes, f–j) large single crystals of calcite formed by the two-step control method, with nucleation triggered with local heating at 180 °C ($\gg T_{ON}$) and then growth sustained at 120 °C, and k–o) polycrystalline calcite crystals formed under ambient conditions. Precursor ACC patterns were formed from solutions comprising $[Ca^{2+}] = 10$ mM, $[Mg^{2+}] = 4$ mM and $[PAA] = 4 \mu\text{g mL}^{-1}$, and possess $T_{ON} = 140$ °C.

main substrates for ACC film deposition. Poly(methyl methacrylate) (PMMA, M_w 130000 g mol^{-1}) and poly(vinyl alcohol) powders (PVA, 98% hydrolyzed, M_w 13000–23000 g mol^{-1}) were purchased from Sigma-Aldrich (UK). PVA aqueous solutions (2% w/w) that are ready for spin-coating were prepared by dissolving 0.2 g PVA powders in 10 mL DI water at 60 °C. NanoBasic TEM grids (NG01-011A) were purchased from Dune sciences. Polydimethylsiloxane (PDMS) was prepared using a SYLGARD 184 silicon elastomer kit.

Fabrication of PDMS Precipitation Wells: A glass master was made by binding a 0.5 cm \times 0.5 cm glass slide of 1 mm thickness to a 2 cm \times 2 cm glass slide with adhesive. Degassed PDMS precursor mixture (10:1 base to catalyst) was poured over a lab-customized glass master and cured in a ventilated oven at 60 °C for 120 min. The cured PDMS was peeled off from the glass master to serve as the PDMS precipitation wells. Gas permeable PDMS films were fabricated by spin-coating 1 mL degassed PDMS precursor liquid on glass at

1000 rpm for 20 sec using Chemat spin-coater (KW-4A), and cured at 60 °C for 120 min.

Deposition of Amorphous Calcium Carbonate (ACC) Thin Films: A few surfaces including glass, silicon <100>, PMMA, PVA, PDMS, and silicon <100> patterned with photoresist were used as substrates for ACC film deposition. The substrates were cut to sizes of 0.5 cm \times 0.5 cm, cleaned with ethanol, dried with N_2 (g), and then treated with air plasma for 15 sec. A substrate was placed at the base of a 1 mm deep PDMS reaction well, which was then covered with a 20 μm thick film of gas-permeable PDMS. 100 μL of a precipitation solution comprising $CaCl_2$ (10 mM), $MgCl_2$ (4–100 mM), and PAA (4 $\mu\text{g mL}^{-1}$) was then injected into the well with syringe and the assembly was placed in a sealed Petri dish containing 2 g of $(NH_4)_2CO_3$ powder. Precipitation of ACC was allowed to proceed for 20 min to 2 h, depending on the concentration of reactants, and the substrate was then washed with ethanol, and dried using a stream of nitrogen gas.

Deposition of Micropatterned ACC: Silicon substrates were patterned using standard photolithography procedures using customized dark-field photomasks (Microlitho LTD, UK). A layer of positive photoresist (MICROPOSIT S1813) was cast on a silicon wafer by spin-coating at 500 rpm for 5 s, followed by 4000 rpm for 30 s, and then soft-baked at 115 °C for 60 s. The photoresist layer was exposed to UV light through a photomask at dose of 150 mJ cm⁻² using a KARL SUSS mask aligner (MJB 3, 350–450 nm), followed by development in MICROPOSIT MF-319 solution for 1 min. The substrate was then washed with DI water and dried with N₂ (g). ACC was then deposited on the micropatterned substrates using the same procedure employed for silicon substrates, followed by a lift-off of photoresist in ethanol for 10 min.

Crystallization of ACC Films with Heating: ACC films were crystallized using a custom-made heating stage with controllable temperatures up to 300 °C. ACC films were heated from room temperature with a ramp rate of 10 °C min⁻¹, and crystallization was monitored by POM under reflection. The temperature at which the ACC films started to nucleate was recorded as the onset nucleation temperature (T_{ON}). Two-step-transformation of the ACC films was carried out by placing a substrate supporting an ACC film on the heating stage at 20 °C below T_{ON}. Nucleation was triggered by gently tapping the ACC film with a heated silver probe (step 1) set at an elevated temperature (>T_{ON}) (see Figure S5, Supporting Information for the set-up). The location of the probe was controlled by a x-y-z displaceable micromanipulator. Crystal growth was then sustained at a temperature below T_{ON} (step 2).

Characterization of Calcium Carbonate Films: The amorphous and crystalline calcium carbonate films were characterized using a range of techniques. The structures of the CaCO₃ films were investigated using POM under reflection (Nikon Eclipse LV100 and Zeiss AXIO Scope A1), while scanning electron microscopy (SEM) was used to image the films. Samples were prepared by mounting the substrates on aluminum stubs with double sided Cu tape, and coating with 2 nm Ir prior to analysis, and the analysis was conducted using a FEI NanoSEM Nova 450 operating at 3 kV.

The structures of the CaCO₃ films were characterized using Transmission Electron Microscopy (TEM). Samples prepared by depositing ACC films on a TEM grid and then heating to induce crystallization were characterized using a FEI Tecnai TF20 FEG-TEM operating at 200 kV. Diffraction patterns were obtained using SAED with apertures of 1 or 5 μm diameters and the electron diffraction patterns were simulated with Singlecrystal software and molecular visualization was carried out using Crystallmaker software. In situ heating experiments were also performed and were carried out using a Gatan single tilt hot stage holder and heater control (SmartSet Model 901). Elemental analysis was carried out with HAADF-STEM and EDX spectroscopy in a FEI Titan3 Themis 300 at 300 kV with HAADF STEM detectors and EDX system.

The thicknesses of the ACC and calcite films were determined by Atomic Force Microscopy (AFM) using a Bruker Multimode 8 with a Nanoscope V controller. Samples of ACC films were scratched to reveal the cross-section, and AFM analyses were conducted over the scratch with contact mode using silicon nitride cantilevers (model SNL-10, Bruker). The amount of Ca and Mg in the ACC precursor films was determined with ICP-OES using a Thermo Fisher Scientific iCAP 7400 radial ICP-OES Analyzer, where samples were prepared by immersing 10 substrates supporting ACC films in 1% HCl solution for 5 min.

Supporting Information

Supporting Information is available from the Wiley Online Library or from the author.

Acknowledgements

This work was supported by funding from the European Research Council (ERC) under the project DYNAMIN, grant agreement number

788968 (S.Z., N.K., and F.C.M.) and an EPSRC Programme Grant that funds the Crystallisation in the Real World Consortium (EP/R018820/1, F.C.M. and Y.Y.K.). The authors thank Mr. Stephen Reid for the ICP-OES analysis and Dr. Mark Holden for the AFM studies. For the purpose of open access, the author has applied a CC-BY public copyright license to any Author Accepted Manuscript (AAM) version arising from this submission.

Conflict of Interest

The authors declare no conflict of interest.

Data Availability Statement

The data that support the findings of this study are openly available in University of Leeds at <https://doi.org/10.5518/1173>, reference number 1.

Keywords

bio-inspired, calcites, crystallization, nonclassical crystallization, polymorphs, solid-state transitions

Received: June 20, 2022

Revised: July 11, 2022

Published online: August 7, 2022

- [1] F. Nudelman, N. A. J. M. Sommerdijk, *Angew. Chem., Int. Ed.* **2012**, *51*, 6582.
- [2] B. Cantaert, D. Kuo, S. Matsumura, T. Nishimura, T. Sakamoto, T. Kato, *ChemPlusChem* **2016**, *82*, 107.
- [3] E. Beniash, J. Aizenberg, L. Addadi, S. Weiner, *Proc. R. Soc. B* **1997**, *264*, 461.
- [4] Y. Politi, T. Arad, E. Klein, S. Weiner, L. Addadi, *Science* **2004**, *306*, 1161.
- [5] A. B. Rodriguez-Navarro, P. Marie, Y. Nys, M. T. Hincke, J. Gautron, *J. Struct. Biol.* **2015**, *190*, 291.
- [6] E. Macias-Sanchez, M. G. Willinger, C. M. Pina, A. G. Checa, *Sci. Rep.* **2017**, *7*, 12728.
- [7] R. T. DeVol, C.-Y. Sun, M. A. Marcus, S. N. Coppersmith, S. C. B. Myneni, P. U. P. A. Gilbert, *J. Am. Chem. Soc.* **2015**, *137*, 13325.
- [8] T. Mass, A. J. Giuffre, C.-Y. Sun, C. A. Stifler, M. J. Frazier, M. Neder, N. Tamura, C. V. Stan, M. A. Marcus, P. U. P. A. Gilbert, *Proc. Natl. Acad. Sci. U. S. A.* **2017**, *114*, E7670.
- [9] A. S. Finemore, M. R. J. Scherer, R. Langford, S. Mahajan, S. Ludwigs, F. C. Meldrum, U. Steiner, *Adv. Mater.* **2009**, *21*, 3928.
- [10] Y.-Y. Kim, N. B. J. Hetherington, E. H. Noel, R. Kroger, J. M. Charnock, H. K. Christenson, F. C. Meldrum, *Angew. Chem., Int. Ed.* **2011**, *50*, 12572.
- [11] J. Aizenberg, D. A. Muller, J. L. Grazul, D. R. Hamann, *Science* **2003**, *299*, 1205.
- [12] F. C. Meldrum, C. O'Shaughnessy, *Adv. Mater.* **2020**, *32*, 2001068.
- [13] A. Gal, K. Kahil, N. Vidavsky, R. T. DeVol, P. U. P. A. Gilbert, P. Fratzi, S. Weiner, L. Addadi, *Adv. Funct. Mater.* **2014**, *24*, 5420.
- [14] E. Loste, R. J. Park, J. Warren, F. C. Meldrum, *Adv. Funct. Mater.* **2004**, *14*, 1211.
- [15] H. Du, C. Courregelongue, J. Xto, A. Bohlen, M. Steinacher, C. N. Borca, T. Huthwelker, E. Amstad, *Chem. Mater.* **2020**, *32*, 4282.
- [16] F. Konrad, F. Gallien, D. E. Gerard, M. Dietzel, *Cryst. Growth Des.* **2016**, *16*, 6310.

- [17] J. T. Han, X. Xu, D. H. Kim, K. Cho, *Chem. Mater.* **2005**, *17*, 136.
- [18] H. F. Gong, M. Pluntke, O. Marti, P. Walther, L. Gower, H. Colfen, D. Volkmer, *Colloids Surf., A* **2010**, *354*, 279.
- [19] C. Li, G. Hong, H. Yu, L. Qi, *Chem. Mater.* **2010**, *22*, 3206.
- [20] X. Cheng, P. L. Varona, M. J. Olszta, L. B. Gower, *J. Cryst. Growth* **2007**, *307*, 395.
- [21] J. T. Han, X. Xu, D. H. Kim, K. Cho, *Adv. Funct. Mater.* **2005**, *15*, 475.
- [22] B. Cantaert, Y.-Y. Kim, H. Ludwig, F. Nudelman, N. A. J. M. Sommerdijk, F. C. Meldrum, *Adv. Funct. Mater.* **2012**, *22*, 907.
- [23] Y. F. Xu, F. Nudelman, E. D. Eren, M. J. M. Wirix, B. Cantaert, W. H. Nijhuis, D. Hermida-Merino, G. Portale, P. H. H. Bomans, C. Ottmann, H. Friedrich, W. Bras, A. Akiva, J. Orgel, F. C. Meldrum, N. Sommerdijk, *Nat. Commun.* **2020**, *11*, 12.
- [24] A. Sugawara, T. Nishimura, Y. Yamamoto, H. Inoue, H. Nagasawa, T. Kato, *Angew. Chem., Int. Ed.* **2006**, *45*, 2876.
- [25] Z. Liu, C. Shao, B. Jin, Z. Zhang, Y. Zhao, X. Xu, R. Tang, *Nature* **2019**, *574*, 394.
- [26] Z. Mu, K. Kong, K. Jiang, H. Dong, X. Xu, Z. Liu, R. Tang, *Science* **2021**, *372*, 1466.
- [27] C. C. Tester, M. L. Whittaker, D. Joester, *Chem. Commun.* **2014**, *50*, 5619.
- [28] J. Aizenberg, A. J. Black, G. M. Whitesides, *Nature* **1999**, *398*, 495.
- [29] B. Cantaert, Y.-Y. Kim, H. Ludwig, F. Nudelman, N. A. J. M. Sommerdijk, F. C. Meldrum, *Adv. Funct. Mater.* **2012**, *22*, 907.
- [30] X. Xu, J. T. Han, K. Cho, *Chem. Mater.* **2004**, *16*, 1740.
- [31] L. B. Gower, D. J. Odom, *J. Cryst. Growth* **2000**, *210*, 719.
- [32] L. B. Gower, *Chem. Rev.* **2008**, *108*, 4551.
- [33] J. Ihli, P. Bots, A. Kulak, L. G. Benning, F. C. Meldrum, *Adv. Funct. Mater.* **2013**, *23*, 1965.
- [34] S. Zhang, O. Nahi, L. Chen, Z. Aslam, N. Kapur, Y.-Y. Kim, F. C. Meldrum, *Adv. Funct. Mater.* **2022**, *32*, 2201394.
- [35] J. K. Berg, T. Jordan, Y. Binder, H. G. Börner, D. Gebauer, *J. Am. Chem. Soc.* **2013**, *135*, 12512.
- [36] N. Koga, Y. Z. Nakagoe, H. Tanaka, *Thermochim. Acta* **1998**, *318*, 239.
- [37] J. Ihli, W. C. Wong, E. H. Noel, Y.-Y. Kim, A. N. Kulak, H. K. Christenson, M. J. Duer, F. C. Meldrum, *Nat. Commun.* **2014**, *5*, 3169.
- [38] A. V. Radha, A. Navrotsky, *Cryst. Growth Des.* **2015**, *15*, 70.
- [39] A. V. Radha, A. Fernandez-Martinez, Y. Hu, Y.-S. Jun, G. A. Waychunas, A. Navrotsky, *Geochim. Cosmochim. Acta* **2012**, *90*, 83.
- [40] G. Wolf, C. Gunther, *J. Therm. Anal. Calorim.* **2001**, *65*, 687.
- [41] M. P. Schmidt, A. J. Illott, B. L. Phillips, R. J. Reeder, *Cryst. Growth Des.* **2014**, *14*, 938.
- [42] M. Faatz, F. Grohn, G. Wegner, *Adv. Mater.* **2004**, *16*, 996.
- [43] D. J. Tobler, J. D. R. Blanco, H. O. Sorensen, S. L. S. Stipp, K. Dideriksen, *Cryst. Growth Des.* **2016**, *16*, 4500.
- [44] Z. Zou, L. Bertinetti, Y. Politi, A. C. S. Jensen, S. Weiner, L. Addadi, P. Fratzl, W. J. E. M. Habraken, *Chem. Mater.* **2015**, *27*, 4237.
- [45] H. Du, M. Steinacher, C. Borca, T. Huthwelker, A. Murello, F. Stellacci, E. Amstad, *J. Am. Chem. Soc.* **2018**, *140*, 14289.
- [46] Z. Liu, Z. Zhang, Z. Wang, B. Jin, D. Li, J. Tao, R. Tang, J. J. De Yoreo, *Proc. Natl. Acad. Sci. U. S. A.* **2020**, *117*, 3397.
- [47] K. L. Beers, J. F. Douglas, E. J. Amis, A. Karim, *Langmuir* **2003**, *19*, 3935.
- [48] K. Taguchi, H. Miyaji, K. Izumi, A. Hoshino, Y. Miyamoto, R. Kokawa, *Polymer* **2001**, *42*, 7443.
- [49] K. Murata, H. Chihara, C. Koike, T. Takakura, Y. Imai, A. Tsuchiyama, *Astrophys. J.* **2009**, *697*, 836.
- [50] J. D. Rodriguez-Blanco, S. Shaw, L. G. Benning, *Nanoscale* **2011**, *3*, 265.
- [51] K. Sawada, T. Ogino, T. Suzuki, *J. Cryst. Growth* **1990**, *106*, 393.
- [52] J. Ihli, W. C. Wong, E. H. Noel, Y. Y. Kim, A. N. Kulak, H. K. Christenson, M. J. Duer, F. C. Meldrum, *Nat. Commun.* **2014**, *5*, 3169.
- [53] L. Yu, M. R. Niazi, G. O. Ngongang Ndjawa, R. Li, A. R. Kirmani, R. Munir, A. H. Balawi, F. Laquai, A. Amassian, *Sci. Adv.* **2017**, *3*, e1602462.
- [54] J. Gautron, L. Stapane, N. L. e Roy, Y. Nys, A. B. Rodriguez-Navarro, M. T. Hincke, *BMC Mol. Cell Biol.* **2021**, *22*, 11.
- [55] K. Kahil, N. Varsano, A. Sorrentino, E. Pereiro, P. Rez, S. Weiner, L. Addadi, *Proc. Natl. Acad. Sci. U. S. A.* **2020**, *117*, 30957.
- [56] Y. Li, W. Cai, G. Duan, *Chem. Mater.* **2008**, *20*, 615.
- [57] L.-B. Mao, H.-L. Gao, H.-B. Yao, L. Liu, H. Colfen, G. Liu, S.-M. Chen, S.-K. Li, Y.-X. Yan, Y.-Y. Liu, S.-H. Yu, *Science* **2016**, *354*, 107.
- [58] X. G. Cheng, L. B. Gower, *Biotechnol. Prog.* **2006**, *22*, 141.
- [59] F. F. Amos, D. M. Sharbaugh, D. R. Talham, L. B. Gower, M. Fricke, D. Volkmer, *Langmuir* **2007**, *23*, 1988.
- [60] J. J. De Yoreo, A. K. Burnham, P. K. Whitman, *Int. Mater. Rev.* **2002**, *47*, 113.
- [61] T. Byrappa, J. Ohachi, *Crystal Growth Technology*, Springer, Berlin, Germany **2002**.
- [62] R. J. Park, F. C. Meldrum, *J. Mater. Chem.* **2004**, *14*, 2291.
- [63] B. Wucher, W. Yue, A. N. Kulak, F. C. Meldrum, *Chem. Mater.* **2007**, *19*, 1111.